Journal of the European Ceramic Society **6** (1990) 39–45

Sintering and Electrical Properties of CaO-doped Y_2O_3

K. Katayama, H. Osawa, T. Akiba

Research and Development Division, Chichibu Cement Co., Ltd, 5310 Mikajiri, Kumagaya-shi, Saitama 360, Japan

&

H. Yanagida

Research Center for Advanced Science and Technology, The University of Tokyo,
Komaba, Meguro-ku, Tokyo 153, Japan

(Received 27 November 1989; revised version received 7 February 1990; accepted 12 February 1990)

Abstract

The sinterability and electrical properties of CaO-doped Y_2O_3 were studied as a function of the CaO concentration. Density increased with the CaO concentration with the maximum density being observed in the sample containing 1 mol% CaO. The electrical conductivity of CaO-doped Y_2O_3 varied according to the amount of the water vapor and oxygen pressures. Transport numbers of the electron hole, proton and oxygen were calculated from electromotive force measurements. These results confirmed that a decrease in electrical conductivity as the water vapor pressure increases is attributed to the decrease in hole conductivity.

Das Sinterverhalten und die elektrischen Eigenschaften von Ca-dotiertem Y_2O_3 wurden als Funktion der CaO-Konzentration untersucht. Die Dichte stieg mit der CaO-Konzentration an, wobei ein Dichtemaximum bei der Probe mit 1 mol% CaO beobachtet wurde. Die elektrische Leitfähigkeit des CaO-dotierten Y_2O_3 änderte sich mit dem Wasserdampfgehalt und dem Sauerstoffdruck. Die Überführungszahlen von Elektronenfehlstellen, der Protonen und Sauerstoffatomen wurden anhand der Messung der elektromotorischen Kräfte berechnet. Diese Ergebnisse bestätigen, daß ein Abfall der elektrischen Leitfähigkeit auftritt, wenn der Wasserdampfdruck ansteigt, was auf den Abfall der Leerstellen-Leitfähigkeit zurückzuführen ist.

On a étudié l'aptitude au frittage et les propriétés électriques de l'Y_2O_3 dopée à la CaO en fonction de la teneur en CaO. La densité augmente avec la quantité de CaO avec une densité maximum pour l'échantillon contenant 1% molaire de CaO. La conductivité électrique de ces matériaux varie en fonction des pressions d'oxygène et de vapeur d'eau. Les nombres de transport de la lacune électronique, du proton et de l'oxygène ont été calculés à partir de mesures de force électromotrice. Ces résultats confirment qu'une décroissance de la conductivité électrique lors d'une augmentation de la pression de vapeur d'eau est imputable à la baisse de conductivité de lacune.

1 Introduction

The effect of water vapor on the electrical conductivity of oxides has been investigated,[1,2] and the application of these oxides to fuel cells[3] or sensing devices[4] has been demonstrated. Such applications utilize the proton conduction generated in the presence of water vapor.

Norby and Kofstad studied the electrical properties of Y_2O_3[1,5,6] and found that the total conductivity of Y_2O_3 could be divided into contributions from electron holes, oxygen ions and protons.[7] They prepared dense samples by using hot-press sintering, because Y_2O_3 is inherently too difficult to sinter densely.

The effect of the addition of divalent oxides on the sinterability and electrical conductivity of Y_2O_3 was studied, and it was found that CaO was the most effective for improving the sinterability and for increasing the electrical conductivity.[8] Furthermore, it was found that the electrical conductivity of Y_2O_3

Journal of the European Ceramic Society 0955-2219/90/$3·50

containing CaO varied according to the amount of the water vapor pressure.

In the present study, the sinterability and electrical conductivity of Y_2O_3 are studied as functions of the CaO concentration (0–10 mol%), and the water vapor pressure dependence of electrical conductivity is investigated in more detail.

2 Experimental

A high-purity yttria powder (99·99% purity, Rare Metallic Co., Ltd, Tokyo, Japan) and an analytical grade calcium nitrate (Kanto Chemical Co., Ltd, Tokyo, Japan) were used in the initial phase. Calcium nitrate was dissolved in distilled water, and 0·05 mol/liter solution was prepared. Required amounts of nitrate solution (1–100 ml) and yttria powder (10·1–11·2 g) were placed in an agate mortar. Ethyl alcohol was poured upon them, followed by air-drying at room temperature. Then the resulting masses were wet-mixed in ethyl alcohol in an agate mortar and pestle for 30 min and dried at 125°C. The dried mixtures were calcined at 1000°C for 1 h and thoroughly pulverized into fine powder. The powder was pressed into pellets (20 mm in diameter) × 2 mm thick) at 50 MPa. The pressed pellets were sintered in air at 1500–1700°C for 5 h. The phases present were identified by using XRD (RAD-B, Rigaku Denki Co., Ltd, Tokyo, Japan) and the lattice constants were determined using ten reflections in the 20–120 2θ range by referring to an internal standard of silicon powder (99·99% purity, Rare Metallic Co., Ltd). The density of the pellets was measured by a weight-and-size calculation. Some pellets were crushed and thoroughly pulverized into fine powder, the density of these powders being carefully measured using the toluene immersion technique. Microstructures were observed using a scanning electron microscope (SIGMA-V, Akashi Beam Technology, Tokyo, Japan) and the average grain size was calculated using an intercept method.

The electrical conductivity (σ) was measured by a frequency of 10 kHz. The pellets were ground to a thickness of 1 mm, and a platinum paste (A-4338, Engelhard, New Jersey, USA) was painted on both sides of the pellets and fired to form porous electrodes. The oxygen pressure dependence of σ was measured in several O_2/N_2 gas mixtures. The water vapor pressure dependence of σ was measured in air. The water vapor pressure was controlled using a humidity generator (SRH-1H, Shinei Co., Ltd, Kobe, Japan).

The electromotive force (EMF) was measured using an electrometer (TR-8641, Advantest, Tokyo, Japan) to evaluate the oxygen ion and proton transport numbers, $t_{O^{2-}}$ and t_{H^+}, respectively. Details of the measurements will be given later.

3 Results and Discussion

3.1 Microstructures

Figure 1 shows the density of the sintered samples. The density increased as the CaO concentration increased, with the maximum density being observed in the sample containing 0·2 mol% CaO when sintered at 1500°C or in the sample containing 1·0 mol% CaO when sintered at 1600 or 1700°C. The density of samples containing 0·5 mol% CaO or more sintered at 1600°C is slightly higher than that of samples sintered at 1700°C. These results indicated that the sinterability of Y_2O_3 was greatly improved by the addition of CaO up to 1 mol%, but an excess amount hardly had any effect.

Figure 2 represents microstructures of samples sintered at 1600°C. For Y_2O_3 without CaO, an interconnected network of open porosity was discernible and a porous structure was clearly observed (Fig. 2(a)). As the concentration of CaO increased, pores became more or less isolated from each other, and concentrated at grain boundaries (Fig. 2(b), (c) and (d)). With further increases in the CaO concentration, isolated pores at grain boundaries disappeared, and the pores located within grains became dominant (Fig. 2(e) and (f)). These results suggested that the higher densities of samples containing 1·0 mol% CaO or more sintered at 1600°C compared to those of samples sintered at 1700°C may be attributed to an increase in intragrain pore size.

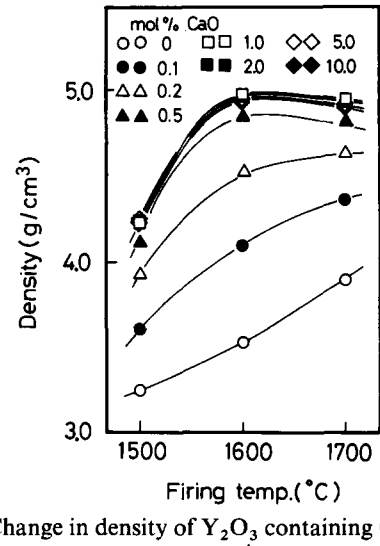

Fig. 1. Change in density of Y_2O_3 containing CaO at various concentrations.

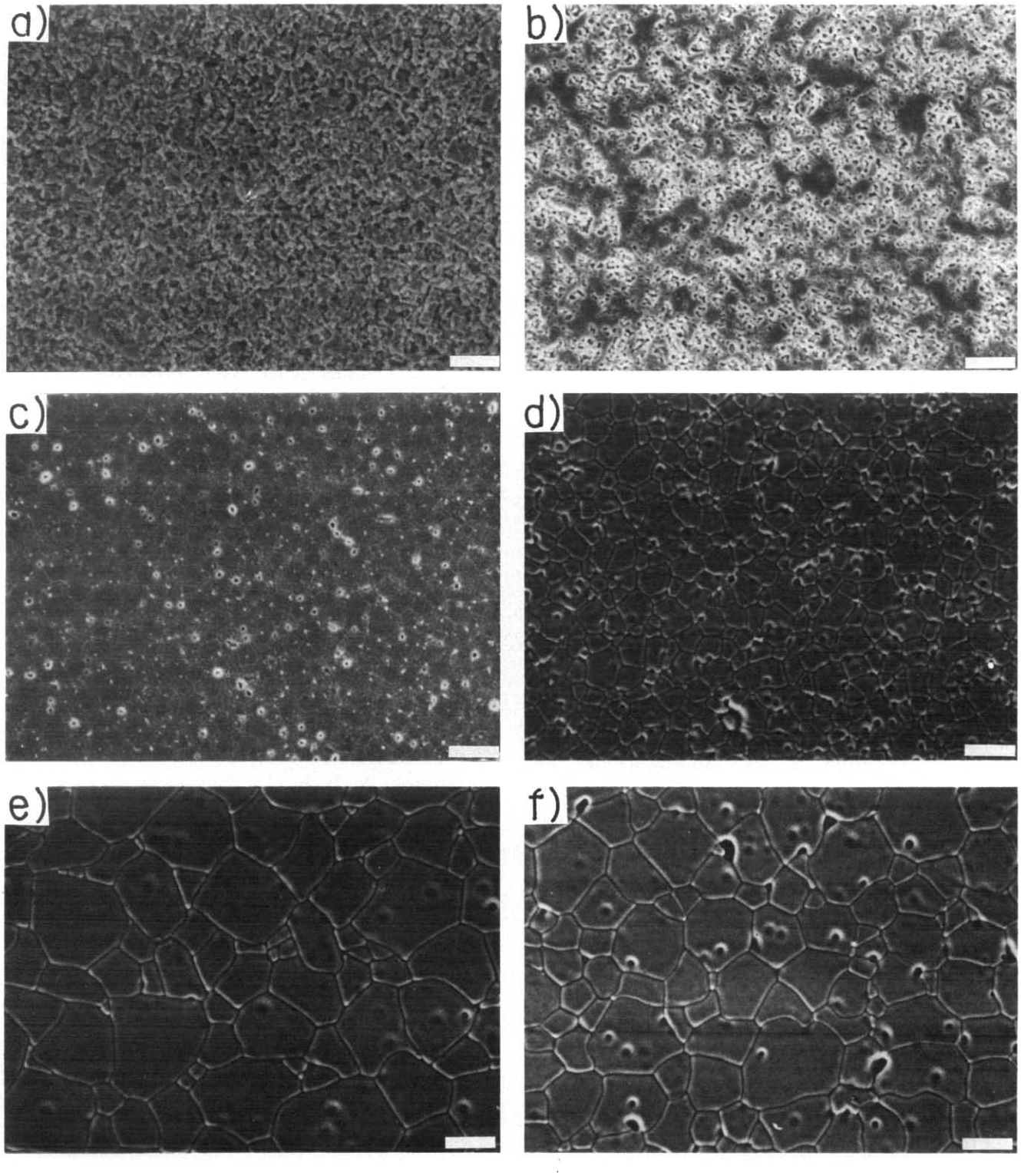

Fig. 2. Microstructures of samples containing (a) 0, (b) 0·1, (c) 0·5, (d) 1·0, (e) 5·0 and (f) 10·0 mol% CaO. Bars = 10 μm.

Figure 3 shows the change in the average grain size of the samples. As can be seen in Fig. 2, the grain size in samples sintered at 1600°C increased with the CaO concentration, with the maximum grain size being observed in the sample containing 5 mol% CaO. A similar tendency was observed in samples sintered at 1700°C. On the other hand, the grain size in samples sintered at 1500°C remained unchanged, irrespective of the CaO concentration. The variation in density was not consistent with the grain size.

All samples investigated were confirmed to be single-phase solid solutions by XRD. Figure 4 shows the lattice parameter of samples sintered at 1600°C as a function of the CaO concentration. An increase in lattice parameter from 1·060 32 ± 0·000 03 nm for pure Y_2O_3 to 1·060 62 ± 0·000 02 nm

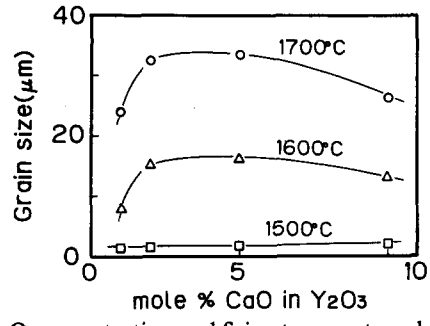

Fig. 3. CaO concentration and firing temperature dependence of grain size.

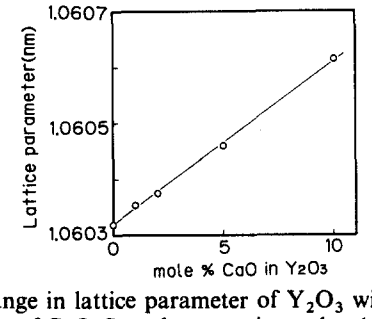

Fig. 4. Change in lattice parameter of Y_2O_3 with increasing concentration of CaO. Samples were sintered at 1600°C for 5 h.

for Y_2O_3 containing 10 mol% CaO is attributed to the substitution of larger Ca^{2+} for the smaller Y^{3+} ions in the lattice. The lattice constant for pure Y_2O_3 was in fair agreement with that measured by Greskovich and O'Clair.[9] EDAX analysis confirmed that CaO was uniformly distributed and segregated neither in the grain boundaries nor around the pores.

3.2 Electrical properties

Figure 5 shows the electrical conductivity (σ) of samples sintered at 1600°C. The measurement was performed in dry air to avoid the influence of water vapor. Electrical conductivity increased with the CaO concentration. The increment in σ became

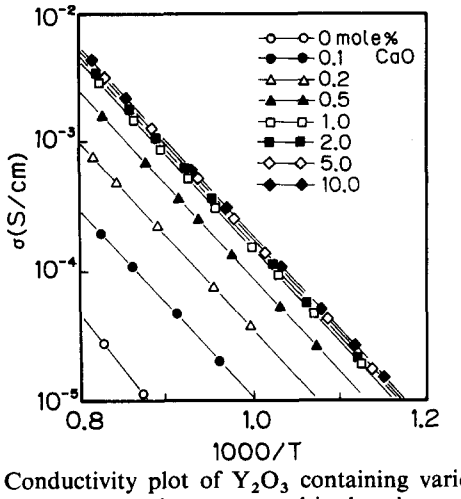

Fig. 5. Conductivity plot of Y_2O_3 containing various CaO concentrations measured in dry air.

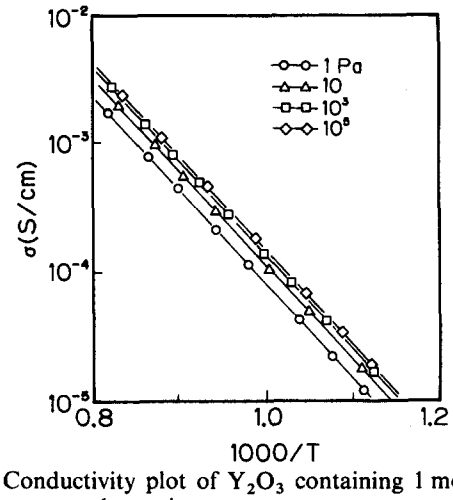

Fig. 6. Conductivity plot of Y_2O_3 containing 1 mol% CaO under various oxygen pressures.

smaller and electrical conductivity remained almost constant when the concentration exceeded 1 mol%.

Figure 6 shows the oxygen pressure dependence of σ for the sample containing 1 mol% CaO sintered at 1600°C measured in a dry atmosphere. The electrical conductivity increased as the oxygen pressure increased. This increase suggested that *p*-type conduction was dominant, and a similar increase was observed even in a wet atmosphere.

Norby and Kofstad[7] have investigated in detail the electrical conductivity of Y_2O_3 and found that the EMF, E, in the system which contains two water vapor pressures ($P_{H_2O}(I)$, $P_{H_2O}(II)$) and two oxygen pressures ($P_{O_2}(I)$, $P_{O_2}(II)$) is given by

$$E = kT/4F[t_{ion} \ln(P_{O_2}(I)/P_{O_2}(II)) - 2t_{H^+} \ln(P_{H_2O}(I)/P_{H_2O}(II))]$$

where t_{ion} and t_{H^+} are transport numbers of native ions and protons, respectively, and native ions include oxygen ions and protons. Thereby, the oxygen ion transport number, $t_{O^{2-}}$, and t_{H^+} can be determined from the following two experiments:

(i) when $P_{O_2}(I) \neq P_{O_2}(II)$ and $P_{H_2O}(I) = P_{H_2O}(II)$, the value of $t_{ion}(= t_{O^{2-}} + t_{H^+})$ can be measured.

(ii) when $P_{H_2O}(I) \neq P_{H_2O}(II) = P_{O_2}(II)$, the value of t_{H^+} can be measured.

Figure 7 shows the EMF of the sample containing 1 mol% CaO sintered at 1600°C measured in a dry atmosphere under condition (i), keeping $P_{O_2}(II) = 10^5$ Pa. As the temperature increased, the EMF decreased, and the linearity was almost preserved in this oxygen range. Thus, the ionic transport number, t_{ion}, at 600, 700 and 800°C could be calculated to be 0·18, 0·09 and 0·04, respectively. A similar measurement was also performed in a wet atmosphere up to $P_{H_2O} = 2 \times 10^3$ Pa.

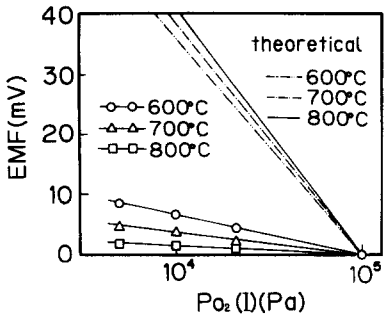

Fig. 7. Plot of EMF versus $P_{O_2}(I)$. $P_{O_2}(II)$ is constant at 10^5 Pa. The theoretical lines correspond to fully ionic transport.

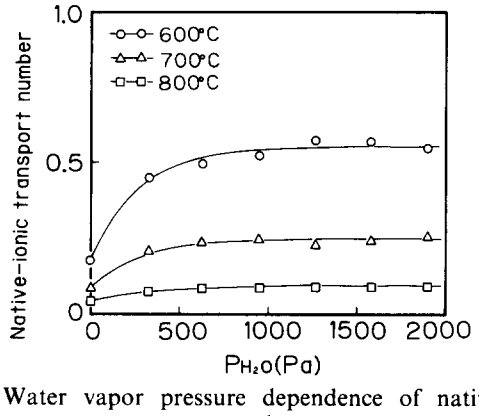

Fig. 8. Water vapor pressure dependence of native ion transport number, t_{ion}.

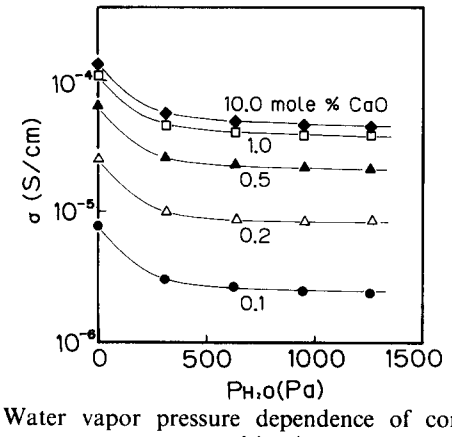

Fig. 9. Water vapor pressure dependence of conductivity measured in air.

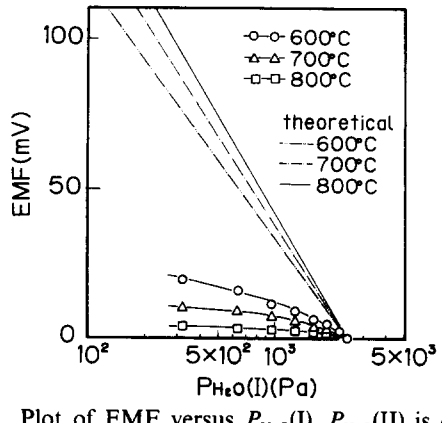

Fig. 10. Plot of EMF versus $P_{H_2O}(I)$. $P_{H_2O}(II)$ is constant at $2{\cdot}5 \times 10^3$ Pa. The theoretical lines correspond to fully ionic transport.

Figure 8 shows the water vapor pressure dependence of t_{ion} for the same sample as that in Fig. 7, which increased as the water vapor pressure increased. Norby and Kofstad already found a similar increase in t_{ion} for pure Y_2O_3.[1] However, t_{ion} became almost constant at a higher temperature and/or at a higher water vapor pressure. These results may be attributed to the dominant *p*-type conduction at higher temperature,[10] and the limited concentration of interstitial oxygen ions which could counterbalance the protons.[6]

Figure 9 shows the water vapor pressure dependence of σ for the same sample as that in Fig. 7 measured in air. Electrical conductivity decreased as the water vapor pressure increased. The similar water vapor pressure dependence of σ was observed in all CaO-doped samples and this humidity-sensitive characteristic was scarcely affected by the CaO concentration. These results indicated that the concentration of interstitial oxygen ion which could counterbalance the protons was limited, but did not increase even though the CaO concentration exceeded 0·1 mol%.

Figure 10 shows the EMF for the same sample as that in Fig. 7 measured in air under condition (ii). The EMF increased as the temperature decreased or as the water vapor pressure, $P_{H_2O}(I)$, decreased. This increase was also attributed to the *p*-type conduction which becomes dominant with increasing temperature or decreasing water vapor pressure which will be discussed below. Anyway, the deviation from the theoretical EMF became large as $P_{H_2O}(I)$ decreased or as the temperature increased. Figure 11 shows the proton transport number, t_{H^+}, which was calculated using the results in Fig. 10. The average pressure, $P_{H_2O,av} = \{P_{H_2O}(I) \cdot P_{H_2O}(II)\}^{1/2}$, was employed as the water vapor pressure.[11] The proton transport number increased as the water vapor pressure increased or as the temperature decreased.

The ionic, hole and proton contributions to the

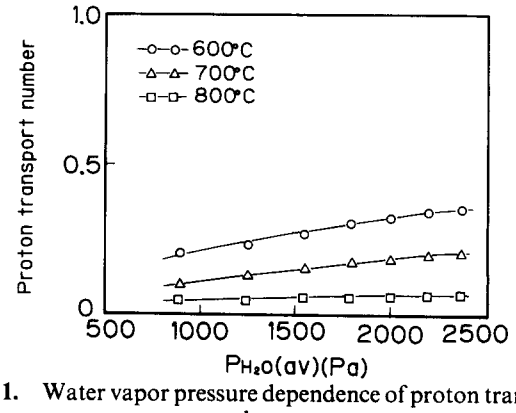

Fig. 11. Water vapor pressure dependence of proton transport number, t_{H^+}.

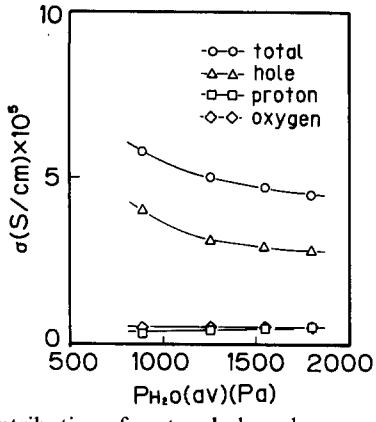

Fig. 12. Contribution of proton, hole and oxygen-ion conductivity to total conductivity of the sample containing 1 mol% CaO sintered at 1600°C.

total conductivity for the sample containing 1 mol% CaO sintered at 1600°C were calculated by the use of transport numbers obtained so far and are shown in Fig. 12. As the vapor pressure increased, the hole conductivity decreased greatly, while the proton conductivity increased slightly and the oxygen conductivity remained almost unchanged. These results reconfirmed that a decrease in total conductivity with increasing water vapor pressure was predominantly caused by a decrease in hole conductivity.[8]

3.3 Effect of CaO doping

The nonstoichiometry of Y_2O_3 at higher oxygen pressures arises from the creation of interstitial oxygen compensated by electron holes:[12]

$$\tfrac{1}{2}O_2(g) \rightleftharpoons O_i'' + 2h^{\cdot} \quad (1)$$

where O″ is doubly negatively charged interstitial oxygen and $h^{\cdot}$ is an electron hole. The introduction of calcium oxides at higher oxygen pressures increases electron holes according to eqn (2)

$$2CaO + \tfrac{1}{2}O_2(g) \rightleftharpoons 2Ca_Y' + 3O_O + 2h^{\cdot} \quad (2)$$

where Ca_Y' and O_O are a Ca^{2+} ion and yttria site and an O^{2-} ion on its regular site respectively. An increase in electrical conductivity with the CaO concentration (Fig. 5) can be interpreted by an increase in hole concentration according to eqn (2).

The proton conduction in oxides was initially observed by Uchida *et al.*, who successfully interpreted the proton conduction in Yb_2O_3-doped $SrCeO_3$ by the use of the following equation:[13]

$$H_2O + 2h^{\cdot} \rightleftharpoons 2H_i^{\cdot} + \tfrac{1}{2}O_2(g) \quad (3)$$

where $H_i^{\cdot}$ denotes a proton in interstitial sites. This equation is also applied in this study. As water vapor pressure increased, the proton concentration increased along with an accompanying decrease in hole concentration according to eqn (3). Then, eqn (1) is shifted to the right, and the concentration of interstitial oxygen ion increases, that is to say, as the water vapor pressure increases, both the proton and interstitial oxygen ion concentrations increase, while the hole concentration decreases. The following eqn (4), which can be obtained by combining eqns (1) and (3), clearly represents the simultaneous formation of protons and interstitial oxygens with the introduction of water vapor.

$$H_2O \rightleftharpoons 2H_i^{\cdot} + O_i'' \quad (4)$$

Each species must maintain the following electroneutrality condition:

$$[H_i^{\cdot}] + [h^{\cdot}] = 2[O_i''] + [Ca_Y'] \quad (5)$$

where [ ] denotes the concentration of each species. The electrical conductivity, σ, is generally given by:

$$\sigma = \sum(ne\mu) \quad (6)$$

where n, e and μ denote the number of charge carriers, the magnitude of the electronic charge and the mobility, respectively. In this case, eqn (6) can be split into the three contributions, namely, those arising from the oxygen ions, the protons and the electron holes:

$$\sigma_{total} = \sigma_O + \sigma_p + \sigma_h \quad (7)$$

$$= -[O_i'']e\mu_O + [H_i^{\cdot}]e\mu_p - [h^{\cdot}]e\mu_h \quad (8)$$

The mobility of electron holes is usually much higher than that of ions ($\mu_h \gg \mu_p, \mu_O$)[14] and, consequently, the following equation may hold:

$$[h^{\cdot}]\mu_h \gg [O_i'']\mu_o, [H_i^{\cdot}]\mu_p \quad (9)$$

It is understood from eqns (8) and (9) that the total conductivity is mainly determined by the hole conductivity, and it decreases as the water vapor pressure increases.

Greskovich and O'Clair[9] studied the sinterability of SrO-doped Y_2O_3 and found that the defects, Sr_Y' and V_o'', accelerate the densification, while either V_o'' or O_i'' accelerate pore removal during sintering. It could be assumed that the oxygen vacancy, V_o'', need not be considered because sintering was done in air in this study. The density would thereby increase with the CaO concentration. An increase in density with CaO was actually observed in Fig. 1. Since eqn (1) was shifted to the left due to an increase in the electron holes when Ca^{2+} substituted Y^{3+} and the concentration of O_i'' decreased, the removal of pores is hindered. Lots of pores were actually observed in the samples containing a higher CaO concentration (Fig. 2).

The density measured by using the sintered samples is usually smaller than the theoretical one because closed pores existed at grain boundaries or within the grains.[15] To measure the density as

Table 1. Density measured using fine powders

CaO in Y_2O_3 (mol%)	*Density (g/cm^3)*			*Theoretical density (g/cm^3)*
	Firing temperature (°C)			
	1500	*1600*	*1700*	
0	5·031	5·028	5·029	5·032
2	5·009	4·996	4·984	5·011

precisely as possible, such pores have to be completely excluded. Pulverizing seemed to be one of the most effective ways to eliminate such pores. Table 1 represents the density measured using fine powders prepared by pulverizing sintered samples. The theoretical density was calculated by assuming the chemical formula of CaO-doped Y_2O_3 as $Y_{2-x}Ca_xO_3$. The density of pure Y_2O_3 was invariable and almost equal to the theoretical one, irrespective of the firing temperature. This was probably because these samples scarcely had any closed pores affecting the density. On the other hand, the density of samples containing 2 mol% CaO decreased and the deviation from the theoretical density increased as the firing temperature increased. This was probably due to residual closed pores which could not be eliminated in spite of being thoroughly pulverized.

4 Conclusions

The sinterability and electrical properties of yttria was investigated as a function of the CaO concentration up to 10 mol%. The sinterability was greatly improved by such an addition although the density of samples containing more than 2·0 mol% CaO decreased due to the formation of intra-grain pores.

The electrical conductivity which increased with the CaO concentration varied greatly with the water vapor pressure. The hole, proton and oxygen contributions to total conductivity were calculated using EMF measurements. These results confirmed that a decrease in electrical conductivity with increasing water vapor pressure was attributed to a decrease in hole conductivity.

Acknowledgments

The authors would like to acknowledge Prof. M. Miyayama, The University of Tokyo, for valuable discussion.

References

1. Norby, T. & Kofstad, P., Electrical conductivity and defect structure of Y_2O_3 as a function of water vapor pressure. *J. Am. Ceram. Soc.*, **67** (1984) 786–92.
2. Iwahara, H., Uchida, H., Ono, K. Ogaki, K., Proton conduction in sintered oxides based on $BaCeO_3$. *J. Electrochem. Soc.*, **135** (1988) 529–33.
3. Iwahara, H., Uchida, H. & Tanaka, S., High temperature-type proton conductive solid oxide fuel cells using various fuels. *J. Appl. Electrochem.*, **16** (1986) 663–8.
4. Nitta, T., Fukushima, F. & Matsuo, Y., Water vapor gas sensor using ZrO_2–MgO ceramic body. In *Chemical Sensors*, ed. T. Seiyama, K. Fueki, J. Shizawa & S. Suzuki. Kodan-sha, Tokyo, 1983, pp. 387–92.
5. Norby, T. & Kofstad, P., Direct-current conductivity of Y_2O_3 as a function of water vapor pressure. *J. Am. Ceram. Soc.*, **69** (1986) 780–3.
6. Norby, T. & Kofstad, P., Electrical conductivity of Y_2O_3 as a function of oxygen partial pressure in wet and dry atmospheres. *J. Am. Ceram. Soc.*, **69** (1986) 784–9.
7. Norby, T. & Kofstad, P., Proton and native-ion conductivities in Y_2O_3 at high temperatures. *Solid State Ionics*, **20** (1986) 169–84.
8. Katayama, K., Osawa, H., Akiba, T., Urabe, K. & Yanagida, H., Sintering of yttrias with addition of divalent metal oxide and water pressure dependence of their electrical conductivity. *J. Mater. Sci.*, **25** (1990) 1503–8.
9. Greskovich, C. & O'Clair, C. R., Transparent, sintered $Y_{2-x}Sr_xO_{3-x/2}$ ceramics. *Adv. Ceram. Mater.*, **1** (1986) 350–5.
10. Schieltz, J., Patterson, J. W. & Wilder, D. R., Electrolytic behavior of yttria. *J. Electrochem. Soc.*, **118** (1971) 1140–4.
11. Uchida, H. & Iwahara, H., Relation between proton and hole conduction in $SrCeO_3$-based solid electrolytes under water-containing atmospheres at high temperatures. *Solid State Ionics*, **11** (1983) 117–24.
12. Gaboriaud, R. J., Self-diffusion of yttrium in monocrystalline yttrium oxide: Y_2O_3. *J. Solid State Chem.*, **35** (1980) 252–61.
13. Uchida, H., Yoshikawa, H. & Iwahara, H., Formation of protons in $SrCeO_3$-based proton conducting oxides. Part I. Gas evolution and absorption in doped $SrCeO_3$ at high temperature. *Solid State Ionics*, **34** (1989) 103–10.
14. Brook, R. J., Defect Structure. In *Electrical Conductivity in Ceramics and Glass*, ed. N. M. Tallan, Marcel Decker Inc., New York, 1974, pp. 250–64.
15. Lowell, S. & Shields, J. E., *Powder Surface Area and Porosity*. Chapman and Hall, London, 1984, pp. 217–24.